31st Congress of the International Council of the Aeronautical Sciences

Belo Horizonte, Brazil; September 09-14, 2018

LONGITUDINAL FLIGHT CONTROL OF BIOINSPIRED FLAPPING-WING MICRO AIR VEHICLE WITH EXTENDED UNSTEADY VORTEX-LATTICE METHOD.

Jong-Wan Lee *, Anh Tuan Nguyen **, Jae-Hung Han*
*** Department of Aerospace Engineering, KAIST, ** Faculty of Aerospace Engineering, Le Quy Don Technical University**

Abstract

This manuscript numerically studies longitudinal flight control of a flapping wing micro air vehicle (FWMAV). In order to consider unsteady aerodynamic effects of the flapping wing motions, the extended unsteady vortex lattice method (UVLM) that includes the leading-edge suction analogy and vortex-growth model was used. The trim search and the linearization of the equations were conducted. Based on the linearized equations, the control gain was obtained by using the LQR method to stabilize hovering and forward flight states. The simulation results shows that the proposed control methodology is effective not only at hovering but also at forward flight with various speeds.

1 Introduction

Flying insects or birds show highly agile flight motions, which conventional micro air vehicles (MAVs) are not able to fully mimic. Flapping wing micro air vehicles (FWMAVs) were invented to mimic the agility of insects and birds. It is well known that flapping wing motion induces complicated unsteady aerodynamic effects, and this complexity should be considered in order to more accurately analyze the flight motions of FWMAV. However, most previous studies on FWMAV control have been conducted using the simplified aerodynamic model [1] or quasi-steady aerodynamic model [2]. Those aerodynamic models cannot consider the unsteady effects such as the wake effect.

The purpose of this study is to construct the control system of an FWMAV in longitudinal direction and to evaluate the designed control systems through more precise simulation using the extended UVLM. The extended UVLM proposed by Nguyen et al. [3] was used as an aerodynamic model in this study. This aerodynamic model can consider the effect of the leading-edge vortices on thin wings and the wing-wake interaction to obtain more accurate and realistic results than the simplified or quasi-steady aerodynamic models. In spite of higher accuracy level, it requires less computation resources and running time than the computational fluid dynamics (CFD) method. The nonlinear dynamic equation was solved using the MSC. Adams software and the aerodynamic force and moment calculations were implemented through user-subroutine functions of the MSC. Adams software. The trimmed flight states for each forward flight speed were obtained using the trim search algorithm proposed by Kim et al.[4] In the trimmed flight states, the linearized equations of motion were obtained as a state-space form. With these trimmed flight states and linearized equations, the optimized control gain was calculated by applying linear quadratic regulator (LQR) method. The feedback control system was constructed with the optimized control gain, and was evaluated through the simulations at various reference speeds (0m/s, 0.6m/s, and 1m/s).

2 Methodology

2.1 FWMAV model.

The FWMAV model used in this study has similar features of hawkmoth *Manduca sexta*, such as mass properties, wing shape and

dimensions. Those features are from the studies of O'Hara et al [5] and Ellington [6]. The wings were assumed to be rigid and massless and the aerodynamic effects on the body were ignored since they are much smaller than the aerodynamics on the wings.

The FWMAV model consists of a body and two wings. In order to systematically describe the motions of the FWMAV, three coordinate systems were defined. The first one is a body-fixed coordinate system [x_b y_b z_b] whose origin is fixed to the center of mass (CM). The x_b of this coordinate system is parallel to the body axis. The second coordinate system [x_G y_G z_G] is fixed to the ground. The last one is a wing-fixed coordinate, which is attached to the wing and the x_w is parallel to the wing span, while the y_w is perpendicular to the wing surface. The stroke plane was set perpendicular to the x_b as most existing FWMAVs. The body pitch angle is denoted here by χ and illustrated in Fig.1.

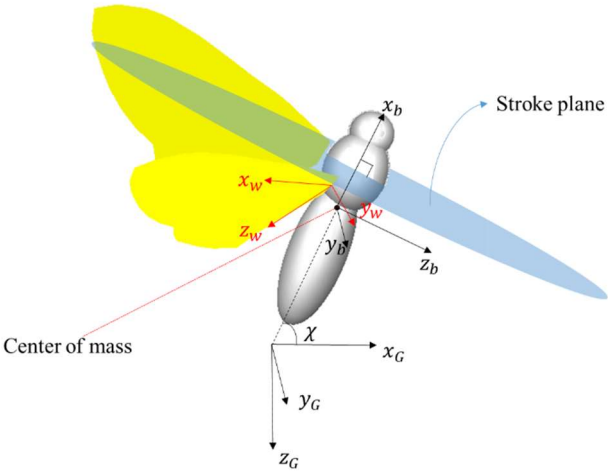

Fig. 1 FWMAV model

2.2 Wing kinematics

The wing kinematic functions used in study is given in Eq. (1). The stroke angle (ϕ) represents the back and forth motion of the wings in the stroke plane. The feathering angle (α) describes the geometric angle of attack. The deviation angle (θ) represents the up and down motion of the wings with respect to the stroke plane.

$$\phi(t) = \phi_{amp}\sin(2\pi ft - \frac{\pi}{2}) + \phi_0$$
$$\alpha(t) = \alpha_0 - \frac{\alpha_{amp}}{\tanh(C_\alpha)}\tanh(C_\alpha\cos(2\pi ft)) + \frac{\pi}{2} \quad (1)$$
$$\theta(t) = 0$$

Here, the components of the wing kinematics except the control parameters were defined as below; the deviation angle was assumed as zero; the ϕ_{amp} and the amplitude of the α_{amp} were set as 50deg and 45deg, respectively. C_α is a constant which was used to define the shape of the feathering angle and set to 2.7 in this study. The wing stroke frequency f, the mean stroke angle ϕ_0, and the mean rotation angle α_0 were chosen to be the control parameters, in this study.

2.3 Aerodynamic Model

The conventional UVLM is based on the potential flow theory, which is valid for the attached and inviscid flows. To complement the conventional UVLM, the leading-edge suction analogy and vortex-core growth model were used.

The leading edge vortices (LEV) on flapping wings is one of the important components providing an extra aerodynamic lift of FWMAVs [7]. In a leading-edge suction analogy model used in the extended UVLM, we assumed that the LEV had a spiral form, similar to that on delta wings, and thus provided an extra normal force component. Eq. (2) shows how the leading-edge suction force F_s is obtained.

$$F_s = \frac{\pi}{16}\frac{\eta_s\rho\Gamma_{L.E.}^{\ 2}}{\Delta x_{L.E.}\cos\Lambda_{L.E.}} \quad (2)$$

where η_s and $\Gamma_{L.E}$ are the coefficient of the leading-edge suction efficiency, and the magnitude of the circulation, respectively. $\Delta x_{L.E}$ and $\Lambda_{L.E}$ are the length and the sweep angle of the local leading-edge panel.

To avoid the singularity problem that may arise when a vortex line is in close proximity with a wing during the wing-wake interaction, each vortex line should have a finite core. Due to this reason, the vortex-core growth model, which

includes the eddy viscosity effect, was adopted. This model is an improved version of the Lamb-Oseen vortex model [8]. Eq. (3) shows the core radius r_c in the vortex-core growth model.

$$r_c = \sqrt{4\alpha_L \nu(1 + a_1 \frac{\Gamma}{\nu})t} \tag{3}$$

Here, the Lamb constant, α_L, was set to 1.25643; ν is the kinematic viscosity; and Squire's parameter, a_1, was set to 0.1 according to Nguyen et al. [3].

Fig. 2 shows the panel mesh on the wing and the wake structures represented as purple sheets. It can be also seen that the wake generated at the prior strokes interacts with the wing.

More details about the extended UVLM are given in Nguyen et al. [3].

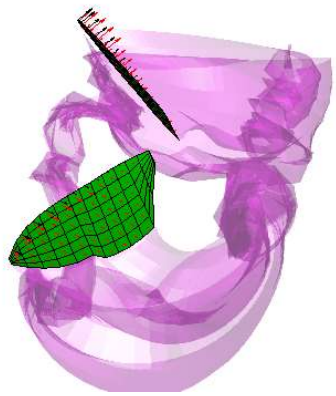

Fig. 2 Flight simulation capture and wake visualization

3. Control system design.

To design an appropriate control system for the FWMAV, the system identification should be done. The trim condition was found at each forward flight speed using a trim search algorithm with non-linear dynamic simulation. At the trim condition, the equation of motion could be linearized and expressed in state-space form. Using the linearized equation, optimal control gain matrix was obtained by using LQR method.

3.1 Equation of motion

$$\begin{aligned} X - mg\sin\chi &= m(\dot{u} + qw) \\ Z + mg\cos\chi &= m(\dot{w} - qu) \\ M &= I_{yy}\dot{q} \end{aligned} \tag{4}$$

Eq. (4) is the 3-DOF nonlinear longitudinal equations of motion of the FWMAV model and was described in body-fixed coordinate system. Here, M is the pitch moment, X and Z are the aerodynamic forces respectively in x and z directions of the body-fixed coordinate. u and w are the velocities in x and z directions of the body-fixed coordinate, respectively. q is the pitch rate of the body.

3.2 Trim search algorithm.

At the trim condition, the FWMAV model slightly oscillates around the equilibrium flight states. In this study, these states were found at each given forward flight speed using the gradient-based trim search algorithm studied by Kim et al [4]. According to the gradient-based trim search algorithm, many simulations are iterated until the trim conditions are satisfied. The initial velocity and offset forces are updated at each iterations to make the model balanced. The control parameters(f, ϕ_0, α_0) were changed to cancel out the offset force by using the inversed matrix of control effectiveness matrix (B), which consists of the partial derivative of aerodynamic force and moment with respect to the control parameters as shown in Eq. (5):

$$B = \begin{bmatrix} \frac{\partial \overline{X_G}}{\partial f} & \frac{\partial \overline{X_G}}{\partial \phi_0} & \frac{\partial \overline{X_G}}{\partial \alpha_0} \\ \frac{\partial \overline{Z_G}}{\partial f} & \frac{\partial \overline{Z_G}}{\partial \phi_0} & \frac{\partial \overline{Z_G}}{\partial \alpha_0} \\ \frac{\partial \overline{M}}{\partial f} & \frac{\partial \overline{M}}{\partial \phi_0} & \frac{\partial \overline{M}}{\partial \alpha_0} \end{bmatrix} \tag{5}$$

3.3 Linearized equation of motion

At the trimmed state where the FWMAV oscillates slightly around the equilibrium flight state, the equation of motion can be linearized by

using the cycle-average and small-disturbance assumptions. Eq. (6) is the matrix form of the linearized equation of motion. Here, the over-bar notation denotes the wingbeat cycle-averaged value. The values with Δ are the difference between the averaged values and the trim reference values. U_∞ denotes the forward flight speed.

$$\begin{bmatrix} \Delta\dot{\bar{u}} \\ \Delta\dot{\bar{w}} \\ \Delta\dot{\bar{q}} \\ \Delta\bar{q} \end{bmatrix} = A \begin{bmatrix} \Delta\bar{u} \\ \Delta\bar{w} \\ \Delta\bar{q} \\ \Delta\bar{\chi} \end{bmatrix} \tag{6}$$

where A is written as

$$A = \begin{bmatrix} \frac{\bar{X}_{\bar{u}}}{m} & \frac{\bar{X}_{\bar{w}}}{m} & \frac{\bar{X}_{\bar{q}}}{m} - \bar{U}_\infty \sin\chi & -g\cos\chi \\ \frac{\bar{Z}_{\bar{u}}}{m} & \frac{\bar{Z}_{\bar{w}}}{m} & \frac{\bar{Z}_{\bar{q}}}{m} + \bar{U}_\infty \cos\chi & -g\sin\chi \\ \frac{\bar{M}_{\bar{u}}}{I_{yy}} & \frac{\bar{M}_{\bar{w}}}{I_{yy}} & \frac{\bar{M}_{\bar{q}}}{I_{yy}} & 0 \\ 0 & 0 & 1 & 0 \end{bmatrix} \tag{7}$$

With the control effectiveness matrix B_u and control input matrix u, the linearized system can be represented in a state-space form as

$$\begin{bmatrix} \Delta\dot{\bar{u}} \\ \Delta\dot{\bar{w}} \\ \Delta\dot{\bar{q}} \\ \Delta q \end{bmatrix} = A \begin{bmatrix} \Delta\bar{u} \\ \Delta\bar{w} \\ \Delta\bar{q} \\ \Delta\bar{\chi} \end{bmatrix} + B_u \begin{bmatrix} \Delta f \\ \Delta\phi_0 \\ \Delta\alpha_0 \end{bmatrix} \tag{8}$$

Or,

$$\dot{X} = AX + B_u u \tag{9}$$

Here, B_u was modified from the B matrix as shown in Eq. (10). The partial derivatives of the aerodynamic force and moment were expressed in the body-fixed coordinate and normalized by mass and inertia of moment in B_u.

$$B_u = \begin{bmatrix} \frac{\partial\bar{X}_b}{\partial f}/m & \frac{\partial\bar{X}_b}{\partial\phi_0}/m & \frac{\partial\bar{X}_b}{\partial\alpha_0}/m \\ \frac{\partial\bar{Z}_b}{\partial f}/m & \frac{\partial\bar{Z}_b}{\partial\phi_0}/m & \frac{\partial\bar{Z}_b}{\partial\alpha_0}/m \\ \frac{\partial\bar{M}_b}{\partial f}/I_{yy} & \frac{\partial\bar{M}_b}{\partial\phi_0}/I_{yy} & \frac{\partial\bar{M}_b}{\partial\alpha_0}/I_{yy} \\ 0 & 0 & 0 \end{bmatrix} \tag{10}$$

3.3 Optimal gain obtained by LQR method

With the linearized equations (Eq. (8)) at each forward flight speed, the optimal gain matrix can be obtained using the LQR method.

By using Matrix P, the solution of the Algebraic Riccati Equation(ARE) (Eq. (11)), the optimal gain matrix can be obtained as Eq. (13), which minimizes the cost function(Eq. (12)).[9] The cost function consists of the state-vector X and control input matrix u and weight matrix Q and R. The Q and R matrices are the weight matrices for the states and the control parameters and they were tuned by trial and error.

$$Q + PA + A^T P = PB_u R^{-1} B_u{}^T P \tag{11}$$

$$J = \int_{T_1}^{T_2} x^T Q x + u^T R u \, dt \tag{12}$$

$$\begin{aligned} u &= -R^{-1} B_u{}^T PX = -KX \\ R^{-1} B_u{}^T P &= K \end{aligned} \tag{13}$$

4 Control simulation and results

In this study, longitudinal flight control simulations at various forward flight speeds (0m/s, 0.6m/s, 1m/s) were conducted.

4.1 Trim search result

The trim conditions were found in each forward flight speed case. Fig. 2 shows the trajectories in one cycle at each trim state. The first plot shows the position of the FWMAV, the second one shows the x and z velocities and the third one shows the pitch angle and the pitch rate in a cycle. The red square points represent the begin, while the pink diamond points represent the end of the cycle. The trajectories of the x and

z velocities, and the body pitch angle and pitch rate show that the FWMAV model slightly oscillates around the reference states and comes back near the initial states. These trajectories signify that the model is in the trim state. Table 1 shows the wing kinematic parameters of each trim conditions.

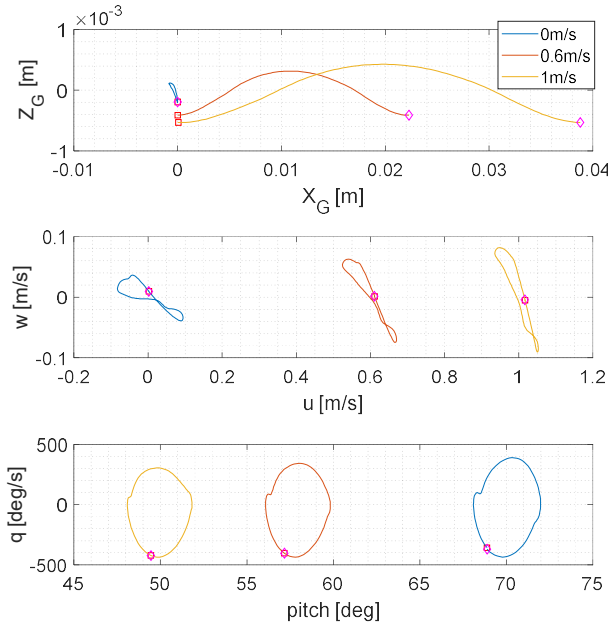

Fig.3 The trajectories in one cycle at trim states

	f(Hz)	ϕ_0(rad)	α_0(rad)
0 m/s	27.89	-0.08922	0.2044
0.6 m/s	26.94	0.1041	0.1959
0.8 m/s	26.35	0.1592	0.1995
1 m/s	25.79	0.2063	0.2051

Table 1 Control parameters at trim conditions

As aforementioned, the equations of motion can be linearized at each forward flight speed and at the same time, the optimal gain matrices can be obtained using the LQR method. For example, the optimal gain matrices **K** for 0m/s, 0.6m/s, 1m/s are shown in Table 2. The matrices K are 3 by 4 matrices and Eq. (14) shows the units of each components of **K**.

$$K = \begin{bmatrix} m^{-1} & m^{-1} & \cdot & s \\ s \cdot m^{-1} & s \cdot m^{-1} & s^{-1} & \cdot \\ s \cdot m^{-1} & s \cdot m^{-1} & s^{-1} & \cdot \end{bmatrix} \quad (14)$$

0m/s				
	1	2	3	4
1	0.05123	-0.02273	1.3334e-04	0.007646
2	-0.06184	-0.1691	-0.01725	-0.04327
3	-0.1998	-0.6023	0.0457	0.8600
0.6m/s				
	1	2	3	4
1	0.02864	-0.08754	-1.781e-03	0.04260
2	-0.04091	-0.3596	-0.01719	-0.04390
3	-0.07522	-0.3906	0.02972	0.7188
1m/s				
	1	2	3	4
1	0.02702	-0.03462	-0.001309	0.02931
2	0.01340	-0.1062	-0.01718	-0.1022
3	-0.1007	-0.07138	0.02948	0.4332

Table 2 Gain matrices K for each forward flight speed

4.2 Control simulation procedure.

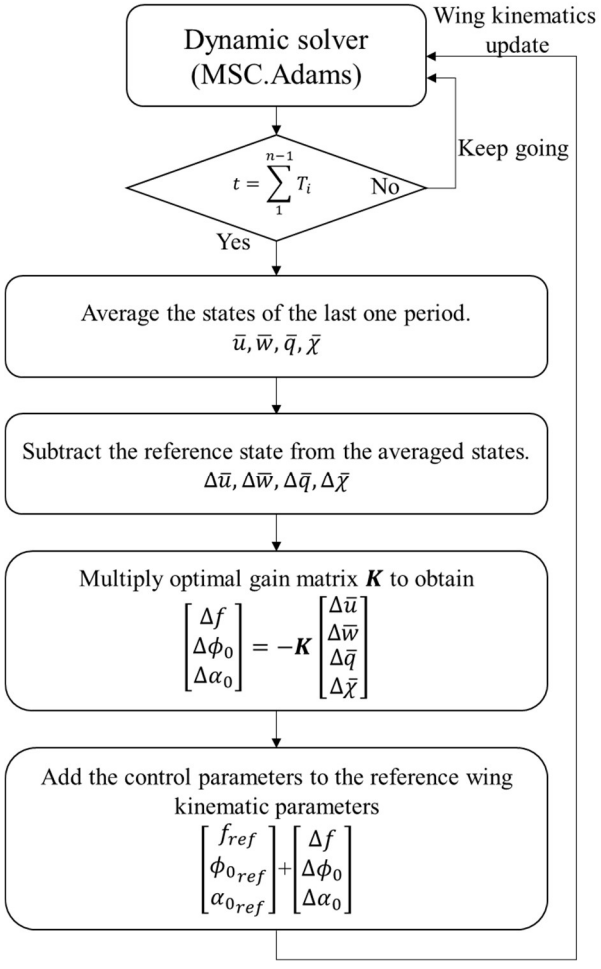

Fig. 4 Flowchart of the control simulation

Fig. 4 shows the whole procedure of the control simulation. Since the equations of motion were linearized using the cycle-averaged method and small disturbance assumptions, there were additional procedures required to calculate the averaged values and disturbance values. The control parameters were updated at the end of each flapping period.

With the initial condition, the dynamic equation were solved using the MSC. ADAMS. At the end of each stroke period, the averaged state values of last period were obtained. Then, the disturbance values were calculated by subtracting the reference states from the averaged states. By using the control gain matrix **K**, the control parameters were updated for the next period.

4.3 Control parameter discontinuity

After updating the control parameters, there may exist discontinuity of the wing kinematics. For example, while the stroke mean angle (ϕ_0) is changed, there is discontinuity between old and new periods in the function of stroke angle as shown in Fig 4. This discontinuity can cause a singularity while calculating aerodynamic force and moment, which is impossible in real flight. To handle this discontinuity problem, a quintic polynomial function (Eq. (15)) whose first and second derivatives are continuous. Here, P represents the set of control parameters. The polynomial function was designed to make the control parameter change smoothly within the quarter of the wing stroke period.

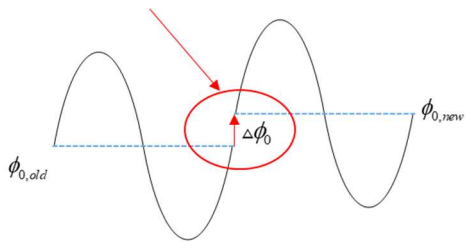

Fig 5 Discontinuity in wing stroke profile

$$h = \begin{Bmatrix} P_{old} & t \le t_0 \\ P_{old} + a(\Delta^3 \cdot [10 - 15\Delta + 6\Delta^2]) & t_0 < t < t_{T/4} \\ P_{new} & t \ge t_{T/4} \end{Bmatrix}$$
$$where\ \Delta = \frac{(t - t_0)}{(t_{T/4} - t_0)} \qquad (15)$$

4.4 Frequent control parameter update

As explained in Sec. 4.2, the control gain was calculated by using the cycle average method. However, updating the control parameters once in a cycle does not guarantee the model to be able to quickly follow the reference. In this study, to make control system react to the disturbance more quickly, we assumed that the control parameters were updated once in a half period, rather in a cycle. It means that the control parameters were updated in the middle of the stroke period and at the end of the stroke period. When they were updated in the middle of the stroke period, the state values from the second half of the past period and the first half of current period were used for averaging.

4.5 Control simulation results and discussion

To evaluate the present designed control system, several simulations were performed. It was assumed that the FWMAV model started to move at a reference forward flight speed, a zero up/down speed, a zero body pitch rate and a reference body pitch angle. Each simulation was run for 2 seconds.

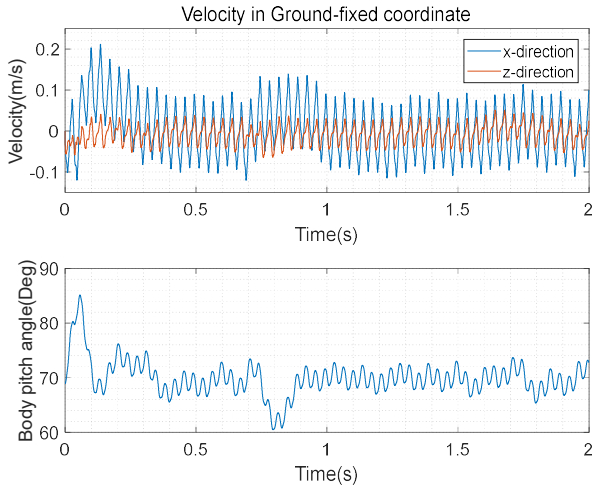

Fig. 6 0m/s control simulation result

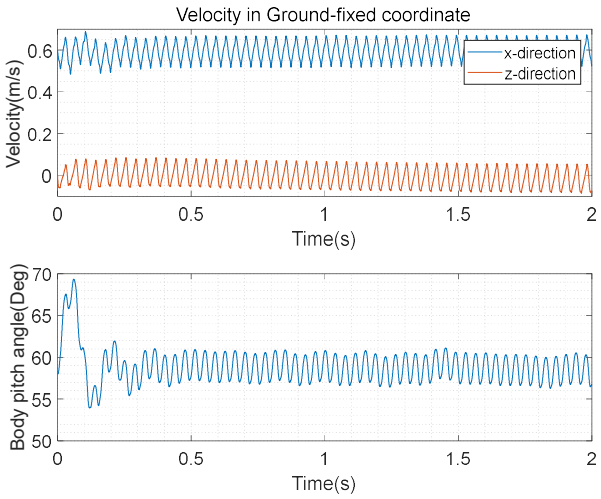

Fig. 7 0.6m/s control simulation result

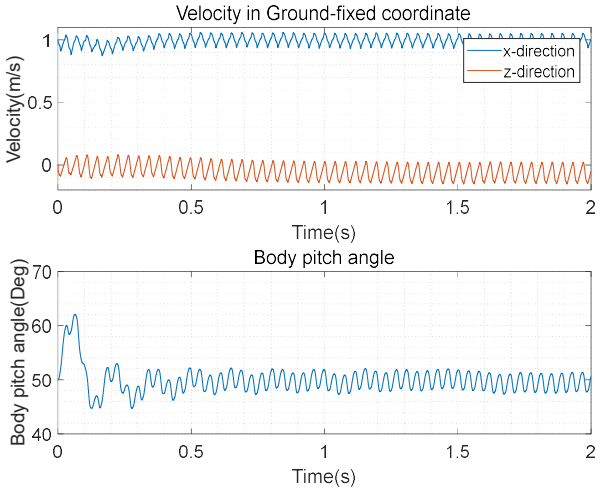

Fig. 8 1m/s control simulation result

Over all, the FWMAV model with control converged to the reference state within 0.5 seconds. There were short transient periods because the given initial conditions are not appropriate to fly in constant speeds. In case of hovering, there was a perturbation that occurs around 0.8 seconds. It seems that there was strong interaction between wake and wings because the model oscillated at the same position and was closed to the wakes. Nevertheless, the control system was still effective and finally the model with control system converged to the reference again.

5 Conclusion

This paper provided the control methodology for FWMAVs together with the simulation results with the extended UVLM. The extended UVLM employed the leading-edge suction analogy and the vortex-core growth method to obtain more accurate aerodynamic force and moment than the simplified aerodynamic model. For the dynamic analysis, the cycle-average and small-disturbance assumptions were used to derive the linearized equations of motion. Based on the dynamic analysis results, the optimal gain was calculated by using LQR method. The control simulation results with the optimal gain matrices show that the control system works well and it is effective in hovering case (0m/s) as well as in forward flight cases(0.6m/s, 1m/s). This result has indicated that the control methodology using the linearization technique is still effective for FWMAV even with strong unsteady aerodynamic effects.

Acknowledgements

This work was supported by the National Research Foundation of Korea(NRF) grant funded by the Korea government(MSIT) (No. NRF-2017R1A2B4005676).

References

[1] Alkitbi M, and Serrani A. Robust control of a flapping-wing mav by differentiable wingbeat modulation. IFAC-PapersOnLine, Vol.49, No.18, pp 290-295, 2016

[2] Bluman J E, Kang C K, Shtessel Y B. Control of a Flapping-Wing Micro Air Vehicle: Sliding-Mode Approach. Journal of Guidance, Control, and Dynamics, Vol.41, No.5, pp1223-1226, 2018

[3] Nguyen A T, Kim J-K, Han J-S and Han J-H. Extended Unsteady Vortex-Lattice Method for Insect Flapping Wings, Journal of Aircraft, Vol. 53, No. 6, pp. 1709-1718, 2016.

[4] Kim J-K, Han J-S, Lee J-S and Han J-H. Hovering and forward flight of the hawkmoth Manduca sexta: trim search and 6-DOF dynamic stability characterization. Bioinspiration & Biomimetics, Vol. 10, No. 5, 20 pp, 2015.

[5] O'Hara R P, Deleon N, and Palazotto A. Structural identification and simulation of a MAV forewing. Composite Structures, Vol. 119, pp 315-321, 2015.

[6] Ellington C P. The Aerodynamics of Hovering Insect Flight. II. Morphological Parameters. Philosophical Transactions of the Royal Society of London. Series B, Biological Sciences, Vol. 305, No. 1122, pp 17–40,1984.

[7] Ellington C P, Van Den Berg C, Willmott A P and Thomas L. R.Leading-Edge Vortices in Insect Flight Nature, Vol. 384, No. 6610,1996, pp. 626–630, 1996.

[8] Ramasamy M, & Leishman J G. A Reynolds Number-Based Blade Tip Vortex Model. Journal of the American Helicopter Society, Vol. 52, No. 3, pp 214-223, 2007.

[9] Burl J B. Linear System Theory,2nd edition, Prentice Hall,1999.

Contact Author Email Address

jaehunghan@kaist.edu

Copyright Statement